

Accepted Manuscript

Title: Effect of SiO₂/Al₂O₃ Ratio on the Performance of Nanocrystal ZSM-5 Zeolite Catalysts in Methanol to Gasoline Conversion

Author: Zhijian Wan Wei Wu Gang Kevin Li Chuanfu Wang
Hong Yang Dongke Zhang



PII: S0926-860X(16)30307-6
DOI: <http://dx.doi.org/doi:10.1016/j.apcata.2016.05.032>
Reference: APCATA 15919

To appear in: *Applied Catalysis A: General*

Received date: 6-3-2016
Revised date: 24-5-2016
Accepted date: 30-5-2016

Please cite this article as: Zhijian Wan, Wei Wu, Gang Kevin Li, Chuanfu Wang, Hong Yang, Dongke Zhang, Effect of SiO₂/Al₂O₃ Ratio on the Performance of Nanocrystal ZSM-5 Zeolite Catalysts in Methanol to Gasoline Conversion, *Applied Catalysis A, General* <http://dx.doi.org/10.1016/j.apcata.2016.05.032>

This is a PDF file of an unedited manuscript that has been accepted for publication. As a service to our customers we are providing this early version of the manuscript. The manuscript will undergo copyediting, typesetting, and review of the resulting proof before it is published in its final form. Please note that during the production process errors may be discovered which could affect the content, and all legal disclaimers that apply to the journal pertain.

**Effect of SiO₂/Al₂O₃ Ratio on the Performance of Nanocrystal ZSM-5
Zeolite Catalysts in Methanol to Gasoline Conversion**

Zhijian Wan, Wei Wu, Gang (Kevin) Li*, Chuanfu Wang, Hong Yang and Dongke Zhang
Centre for Energy (M473), The University of Western Australia, 35 Stirling Highway,
Crawley, WA 6009, Australia

(A manuscript offered to “*Applied Catalysis A: General*”)

* Corresponding author:

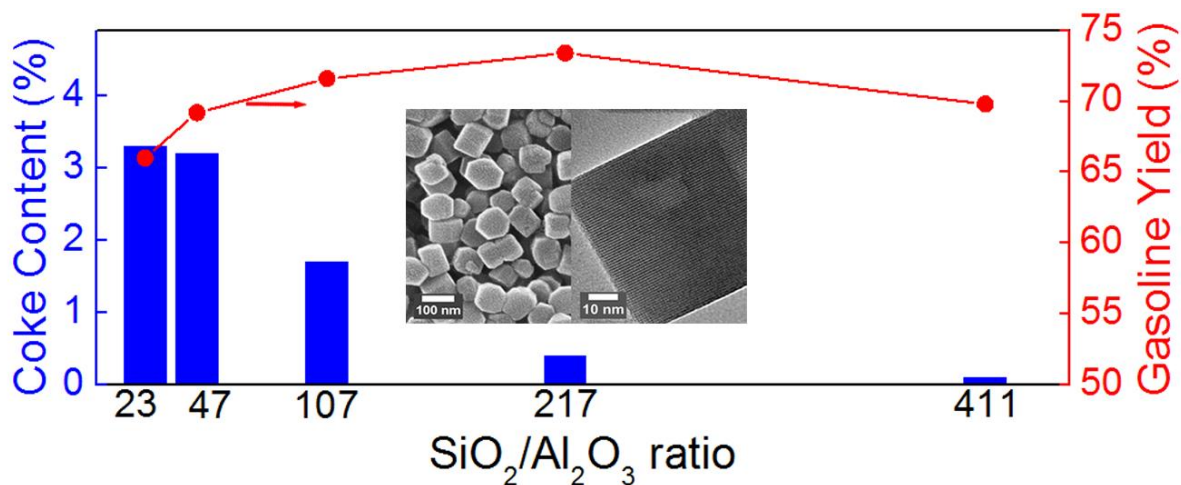
Dr Gang (Kevin) Li

Email: Kevin.li@uwa.edu.au

Phone: +61 8 6488 4636

Fax: +61 8 6488 1024

Graphical abstract

**Highlights**

- Nanocrystal ZSM-5 of different SiO₂/Al₂O₃ ratios but same sizes were obtained
- The effect of SiO₂/Al₂O₃ ratio on methanol to gasoline was systematically studied
- Increasing SiO₂/Al₂O₃ ratio reduced durene yield and improved catalyst durability
- Low SiO₂/Al₂O₃ ratios promoted C₁-C₄ and durene selectivity
- Catalysts with low SiO₂/Al₂O₃ ratios deactivated more rapidly due to coking

Abstract

In this study, the effect of SiO₂/Al₂O₃ ratio on the catalytic performance of nanocrystal ZSM-5 zeolite catalyst in the methanol to gasoline conversion (MTG) was investigated. A series of zeolite samples with different SiO₂/Al₂O₃ ratios of 23, 47, 107, 217 and 411 were synthesised. Through systematically controlling the material synthesis conditions, these nanocrystal ZSM-5 zeolite samples were produced to have very similar crystal sizes and structural properties, thus providing an ideal opportunity to study the intrinsic effect of SiO₂/Al₂O₃ ratio on the performance of the ZSM-5 samples in MTG. The MTG experimentation was carried out in a

fixed-bed reactor under a set of constant conditions of temperature 375 °C, pressure 1 MPa and WHSV 2 h⁻¹. A steady methanol conversion was sustained with increasing the SiO₂/Al₂O₃ ratio, and a progressive decrease in methanol conversion was found over catalysts with low SiO₂/Al₂O₃ ratios (≤ 107) after 5 h on stream. Decreasing the SiO₂/Al₂O₃ ratio promoted C₁-C₄ selectivity and thus decreased gasoline yield. It was also found that decreasing the SiO₂/Al₂O₃ ratio promoted aromatisation reactions and hence higher durene selectivity and more coke formation, resulting in rapid catalyst deactivation. The sample with SiO₂/Al₂O₃ ratio of 217 showed the highest methanol conversion, gasoline yield, and very low coke formation.

Keywords: catalyst deactivation; coke formation; methanol to gasoline; nanocrystal ZSM-5; SiO₂/Al₂O₃ ratio

1. Introduction

Methanol to gasoline (MTG) conversion is one of several promising processes to produce synthetic transport fuel from sources that are independent of the conventional petroleum resource. MTG is a well-known process first discovered in the 1970s by Exxon Mobil [1, 2], which uses methanol as feedstock and ZSM-5 zeolite as catalyst to produce gasoline range hydrocarbons – a sulphur free synthetic liquid fuel with a research octane number (RON) of 90-96, comparable to that of conventional gasoline [3]. Furthermore, the methanol is easy to transport and store, and more importantly, can be made at various scales from various sources such as natural gas, coal and/or biomass [4-7], or even the utilisation of greenhouse gas CO₂ [8], which makes the MTG process attractive.

The most commonly used catalyst for the MTG process is ZSM-5 zeolite. This well-known catalyst has a porous aluminosilicate framework composed by tetrahedral T atoms (T = Si, Al, etc.) connected by oxygen atoms. The framework is negatively charged due to partial

substitution of framework Si by Al, and extra-framework cations (usually Na^+) are used to balance the charge of the unit cells. These cations are ion exchangeable, thus protonated zeolites can be derived by thermally decomposing the ammonium exchanged ones. The proton ions provide strong acid sites which gives ZSM-5 zeolite the high catalytic activity.

As can be inferred from above, the activity of ZSM-5 zeolite is determined by the strength and density of its acid sites, more precisely, the number of accessible Brønsted acid sites per unit cell, which are proportional to the tetrahedrally coordinated Al content in the zeolite framework [9, 10]. Therefore, the $\text{SiO}_2/\text{Al}_2\text{O}_3$ ratio of ZSM-5 zeolite plays an important role in determining its catalytic activity and life span. A ZSM-5 zeolite with high Al content (i.e. low $\text{SiO}_2/\text{Al}_2\text{O}_3$ ratio) generally has high amount of acid sites, and thus high activity. However, the high Al content in a zeolite will also lead to high coke formation rate that results in fast catalyst deactivation [11-13]. This trade-off between the acidity and life span of the ZSM-5 zeolite implies a suitable $\text{SiO}_2/\text{Al}_2\text{O}_3$ ratio is pivotal to ensure the zeolite to have high activity as well as a long life span. A suitable range of $\text{SiO}_2/\text{Al}_2\text{O}_3$ ratio was reported to be 30-70 for micron-sized zeolitic catalysts in MTG conversion [14, 15].

Apart from the intrinsic effect of $\text{SiO}_2/\text{Al}_2\text{O}_3$ ratio, crystal size also impacts greatly on the performance of ZSM-5 catalyst. The ZSM-5 zeolite has three-dimensional microporous channels with 10-membered ring openings with an accessible diameter of 0.55 nm [16-18]. These micropore channels cause diffusion restrictions that make the catalyst prone to coking [19, 20]. The formation of coke subsequently deactivates the catalyst by blocking pore entrances and covering active sites inside the channels [21-23]. This has always been a major concern in industrial applications.

A potentially simple way to overcome diffusion limitations within ZSM-5 zeolite is to reduce its crystal size to the nanoscale, namely, via synthesis of nanocrystal ZSM-5. A reduction in

the crystal size provides ZSM-5 zeolite with increased external surface area, providing more active sites accessible to reactants. More importantly, it greatly shortens the diffusion paths in ZSM-5 nanocrystals, leading to significantly enhanced mass transfer for both reactant and product species to enter and exit the micropores. Nanocrystal ZSM-5 zeolites have been reported to outperform its micron-sized counterparts in various catalytic reactions [24-26]. For example, Rownaghi and co-workers [25] reported a nanocrystal ZSM-5 sample showing long-term catalytic stability, with sustained complete methanol conversion within 10 h on stream, while the methanol conversion of a micron-sized counterpart was only ~65% initially and dropped to 50% during the same reaction time.

The question then arises if nanocrystal ZSM-5 zeolite is used for MTG reaction, will the suitable $\text{SiO}_2/\text{Al}_2\text{O}_3$ ratio be different from that of the conventional micron-sized ZSM-5? To address this question, nanocrystal ZSM-5 of different $\text{SiO}_2/\text{Al}_2\text{O}_3$ ratio but the same crystal size has to be used. However, synthesis of such material is challenging due to the interplay between crystal size and $\text{SiO}_2/\text{Al}_2\text{O}_3$ ratio and, it has not been reported before to the best of our knowledge. In this work, we prepared a series of nanocrystal ZSM-5 zeolites with almost identical crystal size but different $\text{SiO}_2/\text{Al}_2\text{O}_3$ ratios of 23, 47, 107, 217 and 411. Furthermore, we used these materials in MTG reaction to systematically investigate the intrinsic effect of $\text{SiO}_2/\text{Al}_2\text{O}_3$ ratio on the catalyst performance independent of crystal size. X-ray diffraction (XRD), inductively coupled plasma atomic emission spectroscopy (ICP-AES), scanning electron microscopy (SEM), transmission electron microscopy (TEM), solid-state magic angle spinning nuclear magnetic resonance (MAS NMR), ammonia temperature programmed desorption (NH_3 -TPD) and nitrogen physisorption were employed to characterise the structural properties of zeolites. The catalytic performance of the zeolite samples in the MTG conversion was evaluated using a fixed-bed reactor, and coke formation on the used catalysts was analysed using a thermogravimetric analyser (TGA).

2 Experimental

2.1 Reagents

All reagents were purchased from Sigma-Aldrich and used as supplied. These include sodium aluminate (NaAlO_2 , anhydrous, analytic reagent) as the alumina source, tetraethyl orthosilicate (TEOS, $\geq 99.0\%$) as the silica source, and tetrapropylammonium hydroxide (TPAOH, 1.0 M aqueous solution) as the structure directing agent for the synthesis of nanocrystal ZSM-5 zeolites.

2.2 Synthesis of nanocrystal ZSM-5 zeolites

A series of nanocrystal ZSM-5 zeolites with $\text{SiO}_2/\text{Al}_2\text{O}_3$ ratios of 23, 47, 107, 217 and 411 (as determined by ICP-AES) were prepared using a hydrothermal synthesis method, and denoted as NZ_23, NZ_47, NZ_107, NZ_217 and NZ_411, respectively. The samples were synthesised from a sol-gel solution with a molar composition of $x \text{ Na}_2\text{O} : x \text{ Al}_2\text{O}_3 : 100 \text{ SiO}_2 : 25 \text{ TPAOH} : 1157 \text{ H}_2\text{O}$, where x is 4, 2, 1, 0.5 or 0.25, as calculated from a predetermined amount of NaAlO_2 used in the synthesis. The amount of NaAlO_2 used was 0.2 g, 0.1 g, 0.05 g, 0.025 g and 0.0125 g, respectively. For each sample, the predetermined amount of NaAlO_2 and 8 g of 1.0 M aqueous TPAOH solution were added to a 100 mL Schott-Duran bottle and stirred at room temperature for 0.5 h before 6.4 g of TEOS was added drop-wise. The resulting gel was continuously stirred at ambient temperature for 0.5 h, then in an oil bath at 80 °C for 1 h, and finally back to ambient temperature for another 20 h. The prepared gel was transferred to a Teflon-lined autoclave to allow for the hydrothermal reaction at 180 °C for 48 h. After cooling, the sample was collected by centrifugation and washed thoroughly using deionised water three times.

All samples synthesised were dried at 100 °C for 20 h before calcination at 550 °C in air for 5 h to remove the structure directing agent. Ion exchange was then performed to replace Na^+ with NH_4^+ by mixing 1.0 g of sample in 10 mL of 1.0 M NH_4NO_3 solution at 50 °C for 24 h.

The procedure was repeated twice to ensure complete ion exchange. The ion-exchanged samples were again collected by centrifugation and washed in deionised water three times, dried at 100 °C for 20 h and calcined at 500 °C for 5 h to obtain the final H⁺ type ZSM-5 samples.

2.3 Characterisation

Powder XRD was used to verify the structure of the synthesized ZSM-5 zeolite. The XRD patterns were obtained at ambient temperature using a PANalytical Empyrean X-ray diffractometer (Cu K α , $\lambda=1.54439$ Å) at 40 kV and 40 mA, with a scan rate of 2.2° min⁻¹ over a 2 θ range of 5-50°. ICP-AES was used to determine the total SiO₂/Al₂O₃ ratio of the synthesised samples using a Thermo Scientific iCAP 6500 Duo ICP-AES. SEM and TEM images were used to examine the morphology and the sample crystal sizes, with a Zeiss 1555 VP-FESEM instrument (15 kV) and a JEOL 2100 TEM (120 kV), respectively. Solid state MAS NMR was conducted on a Varian 400 wide-bore NMR spectrometer equipped with two radio frequency channels to investigate the coordination of Al in the framework for all samples. ²⁷Al MAS NMR spectra were recorded at 104.2 MHz at a spinning frequency of 5 kHz and 2.05 s intervals between successive accumulations. [Al(H₂O)₆³⁺] was used as the standard reference for ²⁷Al.

In-situ ammonia temperature programmed desorption (NH₃-TPD) was also carried using a Quantachrome ChemBET PULSAR TPR/TPD. Specifically, under high purity helium at a flow rate of 15 mL min⁻¹, approximately 0.1 g of each sample was heated from room temperature at a heating rate of 10 °C min⁻¹ to 500 °C and maintained at this temperature for 60 min to remove any absorbed species. The sample was then cooled down to 120 °C and flushed with a mixture of 5% NH₃ (v/v) in helium at a flow rate of 15 mL min⁻¹ for 40 min. The gas atmosphere was then changed to helium at a flow rate of 15 mL min⁻¹ to remove the

physisorbed NH_3 . After 40 min, the sample was heated again to 650 °C at a heating rate of 10 °C min^{-1} to remove NH_3 absorbed on the acid sites by desorption. The desorbed NH_3 was recorded every 5 s using a thermal conductivity detector (TCD).

The nitrogen adsorption behaviours of the samples were carried out at -196 °C with a Micromeritics Tristar II instrument. Typically, 0.2 g of each sample was degassed under vacuum at 200 °C for 12 h prior to the measurement. The Brunauer-Emmett-Teller (BET) method was used to determine the specific surface area using the adsorption data collected in the pressure range of $p/p_0=0.05-0.2$ [27, 28]. The t-plot method was adopted to calculate the external surface area, micropore area and micropore volume using the adsorption data in the range of $p/p_0=0.2-0.5$ [28]. The total pore volume was estimated from the amount of nitrogen adsorbed at $p/p_0=0.995$.

2.4 Evaluation of Catalytic Performance in MTG

The catalytic performance of the synthesised nanocrystal ZSM-5 catalysts was evaluated in MTG conversion using a high pressure fixed-bed reactor, a schematic of the reactor system is shown in the Supporting Information Figure S1. The as-synthesised ZSM-5 catalyst was pelletised, crushed and sieved into pellets of ~1 mm in diameter. In a typical run, 0.24 g of the catalyst pellets were loaded into the middle section of the reactor – a quartz tube equipped with a stainless steel tube jacket. The reactor was placed in a 400 mm vertical furnace and aligned to ensure the catalyst sit at the centre of the isothermal zone. Prior to the start of the MTG reaction, the catalyst was activated at 375 °C for 2 h under high purity nitrogen purge at a flow rate of 44 mL min^{-1} (STP). Then, liquid methanol (Sigma-Aldrich, HPLC grade, 99.9%) at a flow rate of 0.01 mL min^{-1} was vaporised at 375 °C in a preheater, and then introduced into the reactor using high purity nitrogen as carrier gas at a flow rate of 44 mL min^{-1} , giving a 10% (v/v) methanol in nitrogen mixture. The reactions were allowed to continue for 24 h

under a set of constant conditions of temperature 375 °C, pressure 1 MPa and weight hourly speed velocity (WHSV) 2 h⁻¹.

A split sample of the reactor exit stream was directed to an Agilent 7890A gas chromatograph (GC) and analysed online at a 1 h interval for its composition. To avoid condensation, while the reactor's entire downstream tubes were maintained at 180 °C. The GC was equipped with two capillary columns, VF-1 ms and PoraBOND Q, connected to a thermal conductivity detector (TCD), and three additional capillary columns, CP Ms 5A, CP-Sil 8 CB and PoraBOND Q, connected to a flame ionisation detector (FID). The GC results allowed the calculation of methanol conversion and product selectivity [15, 29, 30].

High catalytic performance should be indicated by high methanol conversion, high gasoline yield and low coke formation. The following naming conventions were used when describing the reaction products: 'C₁-C₄' for the sum of gaseous hydrocarbons with carbon numbers between 1 and 4, namely, C₁-C₄ alkanes and C₂=C₄ alkenes, 'C₅₊ aliphatics' for the sum of liquid nonaromatics, 'aromatics' for the sum of all aromatic products including durene.. The liquid products, namely, all products except C₁-C₄ were considered as gasoline. As C₁-C₄ cannot be used as gasoline and durene affects negatively on gasoline quality, in this study, more attention was paid to the fraction of C₁-C₄ and durene when discussing the product selectivity.

2.5 Coke Analysis

Coking in zeolite catalysed MTG is inevitable. In an effort to peek into the effect of the SiO₂/Al₂O₃ ratio, thus the acidity, of the ZSM-5 zeolite on coke formation and characteristics, TGA analysis was carried out using a SDT600 TGA (TA Instrument) to quantify the coke formed on each spent ZSM-5 zeolite sample after MTG reaction. The TGA measurements were performed with a temperature-programmed heating profile, and were first conducted in

an inert nitrogen atmosphere to vaporise absorbed organic volatiles then followed by air for the coke combustion to quantify coke content in the used catalyst. Typically, under inert nitrogen atmosphere at a flow rate of 100 mL min⁻¹, about 10 mg of a used sample was placed in an alumina crucible. The sample was then heated to 105 °C at a heating rate of 20 °C min⁻¹ and maintained at this temperature for 15 min to remove any surface moisture. The sample was then further heated to 550 °C at a heating rate of 10 °C min⁻¹ and kept at this temperature for 15 min before switching the gas from nitrogen to air, again at a flow rate of 100 mL min⁻¹. The sample was held under air for 40 min to allow for the complete combustion of the coke. The mass loss above 105 °C in nitrogen was ascribed to loss of absorbed volatile residues on the catalyst. The mass loss after switching the gas atmosphere to air was considered to be associated with the combustion of the hard coke formed during the MTG reaction.

3. Results and Discussion

3.1. Strategy of Synthesising nanocrystal ZSM-5 samples with various SiO₂/Al₂O₃ ratios

The synthesis of nanocrystal ZSM-5 samples has been extensively studied and many synthesis methods have been developed. These studies have shown that the crystal size of resultant ZSM-5 zeolite products depends greatly on the precursor composition and synthesis conditions, including factors such as silica and alumina sources, temperature, alkalinity and aging duration of the gel, hydrothermal treatment conditions and SiO₂/Al₂O₃ ratio [31, 32]. Changing SiO₂/Al₂O₃ ratio was observed to have great impact on the crystal size of ZSM-5 zeolite. Generally, an increase in the SiO₂/Al₂O₃ ratio leads to a decrease in the crystal size under otherwise identical conditions [33-35], therefore making it difficult to prepare ZSM-5 zeolites of various SiO₂/Al₂O₃ ratios and similar crystal size from the same method. On the other hand, it is well known that crystal size of the ZSM-5 zeolite can have significant impact on its catalytic performance, particularly on the catalyst deactivation [25, 36]. Thus it is

challenging to investigate the effect of $\text{SiO}_2/\text{Al}_2\text{O}_3$ ratio alone on the catalytic performance of the zeolite and in the past such study has been often performed by ignoring the effect of crystal size [26, 37, 38].

In this study, a simple method was developed to synthesise a series of nanocrystal ZSM-5 samples with various $\text{SiO}_2/\text{Al}_2\text{O}_3$ ratios but almost identical crystal sizes. Changing the $\text{SiO}_2/\text{Al}_2\text{O}_3$ ratios without affecting the crystal sizes of the samples was achieved by varying the amount of the alumina source (NaAlO_2) and using excessive amount of TPAOH, while keeping the amount of other precursor components unchanged. The amount of TPAOH used in the synthesis was relatively high, thus ensuring there was sufficient OH^- in the precursor solutions for all samples. This overrode the effect of varying Al contents on the nuclei formation, and the alkalinity of the gel solutions was almost unaffected. Consequently, nucleation and growth rate of framework structure was not significantly affected during the synthesis when $\text{SiO}_2/\text{Al}_2\text{O}_3$ ratio was varied, enabling the production of ZSM-5 samples with almost identical crystal sizes but of various $\text{SiO}_2/\text{Al}_2\text{O}_3$ ratios.

3.2. Characteristics of nanocrystal ZSM-5 samples with various $\text{SiO}_2/\text{Al}_2\text{O}_3$ ratios

The powder XRD patterns of five synthesised samples are shown in Figure 1. Evidently, these diffraction patterns are almost identical and consistent with that of typical ZSM-5 zeolite reported in the literature [39], confirming that highly crystalline ZSM-5 were produced at all the five different $\text{SiO}_2/\text{Al}_2\text{O}_3$ ratios.

Representative SEM and TEM images of the five samples are shown in Figure 2. All samples consisted of crystals of almost identical size of ~100 nm with a narrow size distribution. The lattice fringes observed along different axis under high resolution TEM further confirmed that each nanocrystal seen in Figure 3 was a high crystalline single crystal with micropore structures of typical ZSM-5 zeolite.

The chemical environment of the framework aluminium in these five samples was verified through ^{27}Al MAS NMR spectra. As shown in Figure 3, the spectrum was dominated with a main resonance peak at ~ 55.5 ppm for all samples and a minor resonance at ~ 0 ppm for the samples with $\text{SiO}_2/\text{Al}_2\text{O}_3$ ratio ≤ 107 . According to the literature [40], the former one can be attributed to the tetrahedrally coordinated Al within the framework structure, whereas the latter one is associated with the octahedrally coordinated Al on the extra framework. Therefore, the majority of the Al in the framework of the synthesised samples was tetrahedrally coordinated, with only a very minor proportion on the extra framework for the samples with low $\text{SiO}_2/\text{Al}_2\text{O}_3$ ratio. The resonance at ~ 0 ppm dropped substantially with increasing $\text{SiO}_2/\text{Al}_2\text{O}_3$ ratio suggesting ZSM-5 zeolites with high Al content (thus low $\text{SiO}_2/\text{Al}_2\text{O}_3$ ratio) are more prone to develop extra framework Al [10, 41].

The acid site distributions of the five samples obtained via NH_3 -TPD are shown in Figure 4. As can be seen, all samples exhibited two well resolved desorption peaks typical of ZSM-5 zeolite, with the low temperature peaks at $150\text{-}320$ °C corresponding to weak acid sites and the high temperature peaks at $320\text{-}550$ °C corresponding to strong acid sites, respectively [42-44]. The intensity of a desorption peak representing the amount of acid sites decreased with increasing $\text{SiO}_2/\text{Al}_2\text{O}_3$ ratio, indicating the amount of acid sites was indeed proportional to the Al content in the catalyst. Clearly, NZ_23 had the highest Al content and thus the highest amount of acid sites, in good agreement with the literature [45, 46]. In this study, a low $\text{SiO}_2/\text{Al}_2\text{O}_3$ ratio was indicative of a high acid site density, and vice versa.

The nitrogen physisorption isotherms of all five samples presented in Figure 5 show all samples exhibited very similar adsorption/desorption behaviour. The steep uptake observed for all isotherms in low relative pressure region ($p/p_0 < 0.01$) reflects a high microporosity in the samples, indicating an intact microporous framework and high crystallinity, consistent with the results of XRD and TEM. The sudden rise in the adsorption capacity at high relative

pressures ($p/p_0 > 0.9$) along with the hysteresis loops suggests the existence of mesopores in the samples. These mesopores were created by intercrystal spaces and are commonly observed in zeolites with nanosized crystals [25, 47]. The adsorption properties of the samples extracted from the isotherms are summarised in Table 1. The BET surface areas, micropore areas and volumes were found to increase slightly (by ~5%) with increasing $\text{SiO}_2/\text{Al}_2\text{O}_3$ ratio, consistent with existing understanding on the aluminium content effect [48, 49]. The total pore volume for all the samples was determined to be $\sim 0.35 \text{ cm}^3 \text{ g}^{-1}$, in good agreement with that of typical nanocrystal ZSM-5 zeolite with high crystallinity [47].

It is clear that for the five ZSM-5 samples produced, although their $\text{SiO}_2/\text{Al}_2\text{O}_3$ ratios varied significantly from 23 to 411, their crystal sizes and structural properties remained almost identical. This thus provided a unique opportunity to independently investigate the effect of $\text{SiO}_2/\text{Al}_2\text{O}_3$ ratio on the catalytic performance of these samples in MTG conversion which is discussed in the following.

3.3 Catalytic performance of nanocrystal ZSM-5 zeolite catalysts

3.3.1 Effect of $\text{SiO}_2/\text{Al}_2\text{O}_3$ ratio on methanol conversion and product distribution

The effect of $\text{SiO}_2/\text{Al}_2\text{O}_3$ ratio on methanol conversion versus time on stream is shown in Figure 6. With the exception of NZ_411, all other ZSM-5 samples showed complete methanol conversion (100%) during the first 5 h reaction period. After that, a decrease in methanol conversion was observed in the samples with low $\text{SiO}_2/\text{Al}_2\text{O}_3$ ratios (NZ_107, NZ_47, NZ_23), and this reduction became increasingly pronounced with decreasing $\text{SiO}_2/\text{Al}_2\text{O}_3$ ratio, indicating the samples having higher aluminium content thus higher acidity were deactivated more rapidly. In addition, the extra framework Al observed for those three samples might also contribute to the fast deactivation [41, 50, 51]. The methanol conversion remained complete and steady for NZ_217 over the 24h time period studied. However, further increasing $\text{SiO}_2/\text{Al}_2\text{O}_3$ ratio to 411 resulted in incomplete methanol conversion (~94%) even from the

very beginning of the reaction. This was most likely due to the reduced number of active sites in NZ_411. As the number of active sites is proportional to the aluminium content in the ZSM-5 zeolite, catalyst with highly increased $\text{SiO}_2/\text{Al}_2\text{O}_3$ ratio of 411 led to insufficiency in active sites and hence incomplete methanol conversion under the reaction conditions enforced. Note that methanol conversion for NZ_217 and NZ_411 remained steady over the reaction time studied, suggesting a sustained catalyst activity on ZSM-5 with high $\text{SiO}_2/\text{Al}_2\text{O}_3$ ratios (due to less coking as elaborated in next section).

The product distributions and gasoline yield of the catalysts with different $\text{SiO}_2/\text{Al}_2\text{O}_3$ ratios are shown in Figure 7. Aromatics decreased with increasing $\text{SiO}_2/\text{Al}_2\text{O}_3$ ratio. The zeolite catalyst with the highest aluminium content (NZ_23) had the highest aromatics selectivity, suggesting a high amount of acid sites clearly promoted the aromatisation reaction. An important effect of increasing $\text{SiO}_2/\text{Al}_2\text{O}_3$ ratio was a significant decrease in the durene selectivity, from 10.8% to 3.9% as $\text{SiO}_2/\text{Al}_2\text{O}_3$ ratio increased from 23 to 411. It was also evident that increasing $\text{SiO}_2/\text{Al}_2\text{O}_3$ ratio facilitated the formation of C_{5+} aliphatics, consequently contributed to an increase in the gasoline yield. The gaseous products $\text{C}_1\text{-C}_4$ that cannot be considered as gasoline, was found to decrease with increasing $\text{SiO}_2/\text{Al}_2\text{O}_3$ ratio.

The term of $\text{C}_1\text{-C}_4$ in this study includes $\text{C}_1\text{-C}_4$ alkanes (paraffins) and $\text{C}_2\text{=C}_4$ alkenes (olefins). The latter, particularly ethylene (C_2H_4) and propylene (C_3H_6), is believed to be the primary products for methanol conversion to hydrocarbons (MTH) catalysed by zeolitic catalysts [52, 53]. Under the reaction conditions for MTG, as demonstrated in the reaction path shown in Figure 8, methanol (CH_3OH) is first catalytically dehydrated to form an equilibrium mixture of dimethyl ether (DME), the mixture undergoes further reactions to form the primary products. These primary products subsequently undergo oligomerisation, cyclisation, aromatisation, aromatic methylation, hydrogen transfer and aromatic dealkylation to form the final product.

The reactions involved in MTH are catalysed by the acid sites arose from the bridging hydroxyl group (Si–OH–Al), shown in Figure 8. Apparently, high amount of acid sites would direct the reactions towards to formation of high hydrocarbons, in agreement with the high aromatic selectivity for NZ_23 discussed above. It also can be inferred that C₂=C₄ alkenes, being the primary products, should have low selectivity at low SiO₂/Al₂O₃ ratio. This is revealed in the selectivity of C₂=C₄ alkenes as a function of SiO₂/Al₂O₃ ratio displayed in Figure 7b, increasing SiO₂/Al₂O₃ ratio led to an increase in C₂=C₄ alkenes. Therefore, a high SiO₂/Al₂O₃ ratio is preferred for the production of light olefins, and is widely reported in the literature for methanol/ethanol to olefins (M/ETO) [37, 54-57].

In contrary, C₁-C₄ alkanes were found to decrease with increasing SiO₂/Al₂O₃ ratio, shown in Figure 7b. This can be understood by the unique shape selectivity of ZSM-5 zeolite [58]. It is well known that ZSM-5 zeolite has an intermediate pore size of ~ 0.55nm, only small and intermediate organic molecules can traverse through these pores [16]. The growth of the molecules formed during the reaction is regulated by the pores, leading to the occurrence of aromatic dealkylation and thus the formation of light hydrocarbons (C₁-C₄). C₂=C₄ alkenes can further react to form other hydrocarbons; however, C₁-C₄ alkanes are saturated and thus relatively stable, remaining as effluent gas. Low SiO₂/Al₂O₃ ratio promoted the further reaction of C₂=C₄ alkenes and also aromatic dealkylation, resulted in C₁-C₄ alkanes being the predominant light hydrocarbons at low SiO₂/Al₂O₃ ratio and the overall C₁-C₄ selectivity decreasing with increasing SiO₂/Al₂O₃ ratio.

Figure 9 shows the product distributions as a function of time on stream for the five catalysts. All the catalysts showed a decrease in the selectivity of C₁-C₄, aromatics and durene, and an increase in C₅₊ aliphatics, reflecting a similar phenomenon as the effect of increasing SiO₂/Al₂O₃ ratio on product distribution. This can be understood by the active sites in the catalysts being progressively covered by coke formed during the reaction, and consequently,

the effective amount of active sites decreased with time on stream. Furthermore, the changes in product distributions with time on stream were found to be more stable for NZ_217 and NZ_411, and more pronounced with decreasing $\text{SiO}_2/\text{Al}_2\text{O}_3$ ratio, indicating a faster coverage of active sites at lower $\text{SiO}_2/\text{Al}_2\text{O}_3$ ratios, in line with the more rapid catalyst deactivation with decreasing $\text{SiO}_2/\text{Al}_2\text{O}_3$ ratio aforementioned.

Overall, NZ_217 had the highest gasoline yield through the course of the test, as a consequence of its complete and steady methanol conversion and relatively low $\text{C}_1\text{-C}_4$ selectivity. It is worth noting that NZ_217 had an acceptable durene selectivity of 4.6%, as durene concentration in the gasoline higher than 5% will cause rough engine operation [3].

3.3.2 Effect of $\text{SiO}_2/\text{Al}_2\text{O}_3$ ratio on coke formation

Deactivation of catalysts is mainly caused by the formation of carbonaceous residues and subsequent deposition on the catalyst surfaces and/or pores, thus covering the active sites. These carbonaceous residues are commonly known as coke, constituting polycyclic aromatic hydrocarbons [22]. During the catalytic reaction, coke is gradually formed and retained in the catalyst. A small proportion of volatile compounds are also trapped in the catalyst thus not considered as “real coke” but the precursors [59]. Therefore, specifically quantifying the “real coke” was studied by thermal gravimetric analysis conducted first in an inert nitrogen atmosphere below 550 °C to remove volatile molecules and then followed by in air for the combustion of the “real coke”.

The weight loss curves of the spent catalysts are shown in Figure 10. It can be found the amount of coke on the spent catalysts was 3.3, 3.2, 1.7, 0.4 and 0.1 wt% for NZ_23, NZ_47, NZ_107, NZ_217 and NZ_411, respectively, after subtracting the trapped volatile components. It is also noticed that the proportion of volatile compounds relative to the total removable organics/coke was more significant for catalysts with higher $\text{SiO}_2/\text{Al}_2\text{O}_3$ ratios,

e.g. around 80% of the removals in the spent NZ_411 sample was volatile compounds whereas only about 25% in NZ_23. Evidently, catalysts with lower $\text{SiO}_2/\text{Al}_2\text{O}_3$ ratios were more prone to coke formation, suggesting samples with high aluminium content would deactivate more rapidly, which was clearly reflected by the time-dependent methanol conversion results shown in Figure 6. In addition, typical SEM and TEM images (Figure S2) of the spent catalysts revealed virtually identical morphologies as their pristine counterparts, suggesting coking was the dominant cause of catalyst deactivation. NZ_217 showed higher sustained activity towards methanol conversion, desirable product selectivity and also the highest gasoline yield. It was also expected that NZ_217 would have longer life span due to its relatively low coke formation. Collectively, the analysis of the five samples showed the one with relatively high $\text{SiO}_2/\text{Al}_2\text{O}_3$ ratio (217) had the best overall catalytic performance. In comparison, previous studies reported a preferred $\text{SiO}_2/\text{Al}_2\text{O}_3$ ratio of 30-70 for zeolitic catalysts in MTG conversion [14, 15]. This difference is actually a reflection of the effect of crystal size on catalytic performance of ZSM-5 zeolite. The earlier studies were based on conventional ZSM-5 zeolites that had crystal size in the micrometre range, in which a certain proportion of active sites were inaccessible to reactants due to its long diffusion path. Thus high Al content (low $\text{SiO}_2/\text{Al}_2\text{O}_3$ ratio) was required for micron-sized ZSM-5 zeolite to provide sufficient accessible active sites to enable good methanol conversion. In contrast, by reducing the crystal size of the zeolite from micron to nanometre scale, the number of accessible active sites is greatly increased leading to higher activity of nanocrystal ZSM-5 zeolite than its conventional counterpart. In other words, nanocrystal ZSM-5 zeolite with the same aluminium content as a micron-sized counterpart would show better catalytic performance [36, 60].

4. Conclusions

An unbiased study of the effect of $\text{SiO}_2/\text{Al}_2\text{O}_3$ ratio on the catalytic performance of nanocrystal ZSM-5 in the MTG conversion at a high pressure (1 MPa) was systematically conducted. Five nanocrystal ZSM-5 samples with different $\text{SiO}_2/\text{Al}_2\text{O}_3$ ratios ranging from 23 to 411 but of similar crystal sizes and structural properties were successfully synthesised. This allowed for the investigation into the intrinsic effect of $\text{SiO}_2/\text{Al}_2\text{O}_3$ ratio on catalytic performance of ZSM-5 zeolite in MTG.

The catalytic performance of the synthesised samples in MTG reaction was examined in a fixed bed reactor. It was shown that decreasing $\text{SiO}_2/\text{Al}_2\text{O}_3$ ratio facilitated higher methanol conversion whereas the catalyst activity was better sustained with increasing $\text{SiO}_2/\text{Al}_2\text{O}_3$ ratio. $\text{C}_2=\text{C}_4$ alkenes decreased and $\text{C}_1\text{-C}_4$ alkanes increased with decreasing $\text{SiO}_2/\text{Al}_2\text{O}_3$ ratio, leading to an increase in the overall $\text{C}_1\text{-C}_4$ selectivity and thus low gasoline yield. Decreasing $\text{SiO}_2/\text{Al}_2\text{O}_3$ ratio also promoted aromatisation reaction, thus high durene selectivity and coke formation, leading to rapid catalyst deactivation. The nanocrystal catalyst with a moderate $\text{SiO}_2/\text{Al}_2\text{O}_3$ ratio of 217 showed a sustained 100% methanol conversion, high gasoline yield and low coke formation under the reaction conditions studied. By using nanocrystal ZSM-5 catalyst in MTG at high pressures, the preferred $\text{SiO}_2/\text{Al}_2\text{O}_3$ ratio is much higher than that for the microcrystal counterparts.

Acknowledgment

Partial financial support has been received for this research from the Australian Research Council under the ARC Linkage Projects Scheme (LP100200136) and Chevron Energy Technology Pty Ltd. The authors also acknowledge the facilities, and the scientific and technical assistance of the Australian Microscopy & Microanalysis Research Facility at the Centre for Microscopy, Characterisation & Analysis, The University of Western Australia, a facility funded by the University, State and Commonwealth Governments. Zhijian Wan also acknowledges the ARC for providing an APAI scholarship.

References

- [1] C.D. Chang, A.J. Silvestri, *J. Catal.* 47 (1977) 249-259.
- [2] N.R.C.F. Machado, V. Calsavara, N.G.C. Astrath, A. Medina, M.L. Baesso, *Appl. Catal. A*. 311 (2006) 193-198.
- [3] C.D. Chang, J.C. Kuo, W.H. Lang, S.M. Jacob, J.J. Wise, A.J. Silvestri, *Ind. Eng. Chem. Process Des. Dev.* 17 (1978) 255-260. 17 (1978) 255-260.
- [4] G.A. Olah, *Angew. Chem. Int. Ed.* 44 (2005) 2636-2639.
- [5] Z.X. Di, C. Yang, X.J. Jiao, J.Q. Li, J.H. Wu, D.K. Zhang, *Fuel*. 104 (2013) 878-881.
- [6] M. Inaba, K. Murata, I. Takahara, K.i. Inoue, *J. Chem. Technol. Biot.* 86 (2011) 95-104.
- [7] A.G. Gayubo, A. Alonso, B. Valle, A.T. Aguayo, J. Bilbao, *Appl. Catal. B*. 97 (2010) 299-306.
- [8] G.A. Olah, A. Goeppert, G.K.S. Prakash, *J. Org. Chem.* 74 (2009) 487-498.
- [9] A. Corma, *J. Catal.* 216 (2003) 298-312.
- [10] A. Primo, H. Garcia, *Chem. Soc. Rev.* 43 (2014) 7548-7561.
- [11] M. Yamamura, K. Chaki, T. Wakatsuki, H. Okado, K. Fujimoto, *Zeolites*. 14 (1994) 643-649.
- [12] M. Li, Y. Zhou, C. Ju, Y. Fang, *Appl. Catal. A*. 512 (2016) 1-8.
- [13] D.M. Bibby, R.F. Howe, G.D. Mclellan, *Appl. Catal. A*. 93 (1992) 1-34.
- [14] C. Chang, S. Grover, US Patent 4,058,576, 1977.
- [15] N.L. Michels, S. Mitchell, J. Perez-Ramirez, *Acs. Catal.* 4 (2014) 2409-2417.
- [16] A.W. Chester, E.G. Derouane, *Zeolite characterization and catalysis*, Springer, Berlin, 2009.
- [17] D.H. Olson, G.T. Kokotailo, S.L. Lawton, W.M. Meier, *J. Phys. Chem.* 85 (1981) 2238-2243.
- [18] R.C. Wei, H. Yang, D.K. Zhang, *Rsc. Adv.* 5 (2015) 63765-63776.

- [19] M. Bjorgen, F. Joensen, M.S. Holm, U. Olsbye, K.P. Lillerud, S. Svelle, *Appl. Catal. A*. 345 (2008) 43-50.
- [20] M. Inaba, K. Murata, M. Saito, I. Takahara, *React. Kinet. Catal. Lett.* 88 (2006) 135-142.
- [21] G.F. Froment, J. Demeyer, E.G. Derouane, *J. Catal.* 124 (1990) 391-400.
- [22] P.L. Benito, A.G. Gayubo, A.T. Aguayo, M. Olazar, J. Bilbao, *Ind. Eng. Chem. Res.* 35 (1996) 3991-3998.
- [23] F. Schmidt, C. Hoffmann, F. Giordano, S. Bordiga, P. Simon, W. Carrillo-Cabrera, S. Kaskel, *J. Catal.* 307 (2013) 238-245.
- [24] M. Choi, K. Na, J. Kim, Y. Sakamoto, O. Terasaki, R. Ryoo, *Nature*. 461 (2009) 246-249.
- [25] A.A. Rownaghi, J. Hedlund, *Ind. Eng. Chem. Res.* 50 (2011) 11872-11878.
- [26] T. Tago, H. Konno, M. Sakamoto, Y. Nakasaka, T. Masuda, *Appl. Catal. A*. 403 (2011) 183-191.
- [27] J.C. Groen, L.A.A. Peffer, J. Perez-Ramirez, *Micropor. Mesopor. Mat.* 60 (2003) 1-17.
- [28] S. Lowell, *Characterization of porous solids and powders: surface area, pore size and density*, Springer, Berlin, 2004.
- [29] Z.J. Wan, W. Wu, W. Chen, H. Yang, D.K. Zhang, *Ind. Eng. Chem. Res.* 53 (2014) 19471-19478.
- [30] K. Kim, R. Ryoo, H.D. Jang, M. Choi, *J. Catal.* 288 (2012) 115-123.
- [31] C.S. Cundy, P.A. Cox, *Chem. Rev.* 103 (2003) 663-701.
- [32] C.S. Cundy, P.A. Cox, *Micropor. Mesopor. Mat.* 82 (2005) 1-78.
- [33] R. Van Grieken, J.L. Sotelo, J.M. Menendez, J.A. Melero, *Micropor. Mesopor. Mat.* 39 (2000) 135-147.
- [34] Y. Wang, L.F. Guo, Y. Ling, Y.M. Liu, X.A.H. Li, H.H. Wu, P. Wu, *Appl. Catal. A*. 379 (2010) 45-53.

- [35] Y.Y. Hu, C. Liu, Y.H. Zhang, N. Ren, Y. Tang, *Micropor. Mesopor. Mat.* 119 (2009) 306-314.
- [36] A.A. Rownaghi, F. Rezaei, J. Hedlund, *Catal. Commun.* 14 (2011) 37-41.
- [37] F.L. Bleken, S. Chavan, U. Olsbye, M. Boltz, F. Ocampo, B. Louis, *Appl. Catal. A.* 447 (2012) 178-185.
- [38] D.B. Lukyanov, *Zeolites.* 12 (1992) 287-291.
- [39] M.M. Treacy, J.B. Higgins, R. von Ballmoos, I.Z. Association, S. Commission, *Collection of simulated XRD powder patterns for zeolites*, Elsevier, New York, 1996.
- [40] O.H. Han, C.S. Kim, S.B. Hong, *Angew. Chem. Int. Ed.* 41 (2002) 469-472.
- [41] K. Barbera, F. Bonino, S. Bordiga, T.V.W. Janssens, P. Beato, *J. Catal.* 280 (2011) 196-205.
- [42] Z.X. Song, A. Takahashi, I. Nakamura, T. Fujitani, *Appl. Catal. A.* 384 (2010) 201-205.
- [43] M. Inaba, K. Murata, I. Takahara, K. Inoue, *Adv. Mater. Sci. Eng.* 2012 (2012).
- [44] M. Inaba, K. Murata, M. Saito, I. Takahara, *Green Chem.* 9 (2007) 638-646.
- [45] D. Ma, W. Zhang, Y. Shu, X. Liu, Y. Xu, X. Bao, *Catal. Lett.* 66 (2000) 155-160.
- [46] A.S. Al-Dughaiter, H. de Lasa, *Ind. Eng. Chem. Res.* 53 (2014) 15303-15316.
- [47] H.B. Zhang, Y.C. Ma, K.S. Song, Y.H. Zhang, Y. Tang, *J. Catal.* 302 (2013) 115-125.
- [48] L. Shirazi, E. Jamshidi, M.R. Ghasemi, *Cryst. Res. Technol.* 43 (2008) 1300-1306.
- [49] A.F.P. Ferreira, M.C. Mittelmeijer-Hazeleger, J.V.D. Bergh, S. Aguado, J.C. Jansen, G. Rothenberg, A.E. Rodrigues, F. Kapteijn, *Micropor. Mesopor. Mat.* 170 (2013) 26-35.
- [50] Z.X. Qin, L. Lakiss, L. Tosheva, J.P. Gilson, A. Vicente, C. Fernandez, V. Valtchev, *Adv. Funct. Mater.* 24 (2014) 257-264.
- [51] K.S. Triantafyllidis, A.G. Vlessidis, L. Nalbandian, N.P. Evmiridis, *Micropor. Mesopor. Mat.* 47 (2001) 369-388.
- [52] S. Ilias, A. Bhan, *Acs. Catal.* 3 (2013) 18-31.

- [53] J. Kim, M. Choi, R. Ryoo, *J. Catal.* 269 (2010) 219-228.
- [54] Z.X. Song, A. Takahashi, N. Mimura, T. Fujitani, *Catal. Lett.* 131 (2009) 364-369.
- [55] C.D. Chang, C.T.W. Chu, R.F. Socha, *J. Catal.* 86 (1984) 289-296.
- [56] D. Goto, Y. Harada, Y. Furumoto, A. Takahashi, T. Fujitani, Y. Oumi, M. Sadakane, T. Sano, *Appl. Catal. A.* 383 (2010) 89-95.
- [57] K. Murata, M. Inaba, I. Takahara, *J. Jpn. Pet. Inst.* 51 (2008) 234-239.
- [58] V. Calsavara, M.L. Baesso, N.R.C. Fernandes-Machado, *Fuel.* 87 (2008) 1628-1636.
- [59] H. Schulz, *Catal. Today.* 154 (2010) 183-194.
- [60] S.K. Saxena, N. Viswanadham, A.a.H. Al-Muhtaseb, *J. Ind. Eng. Chem.* 20 (2014) 2876-2882.

Figure Captions

- Figure 1 Typical XRD patterns of nanocrystal ZSM-5 samples with various $\text{SiO}_2/\text{Al}_2\text{O}_3$ ratios ranging from 23 – 411
- Figure 2 Typical SEM and TEM images of nanocrystal ZSM-5 samples with various $\text{SiO}_2/\text{Al}_2\text{O}_3$ ratios ranging from 23 – 411
- Figure 3 ^{27}Al MAS NMR spectra of nanocrystal ZSM-5 samples with various $\text{SiO}_2/\text{Al}_2\text{O}_3$ ratios ranging from 23 – 411
- Figure 4 NH_3 -TPD profiles of nanocrystal ZSM-5 samples with various $\text{SiO}_2/\text{Al}_2\text{O}_3$ ratios ranging from 23 – 411
- Figure 5 Nitrogen physisorption isotherms of nanocrystal ZSM-5 samples with various $\text{SiO}_2/\text{Al}_2\text{O}_3$ ratios ranging from 23 – 411. Solid symbols denote adsorption and hollow ones for desorption
- Figure 6 Effect of $\text{SiO}_2/\text{Al}_2\text{O}_3$ ratio on methanol conversion of nanocrystal ZSM-5 zeolite catalysts tested at 375 °C, 1 MPa and WHSV of 2 h^{-1}
- Figure 7 Effect of $\text{SiO}_2/\text{Al}_2\text{O}_3$ ratio on product distribution and gasoline yield of nanocrystal ZSM-5 zeolite catalysts tested at 375 °C, 1 MPa and WHSV of 2 h^{-1}
- Figure 8 Proposed reaction pathways for methanol conversion on ZSM-5 catalyst
- Figure 9 Product selectivity as a function of time for the nanocrystal ZSM-5 zeolite catalysts with various $\text{SiO}_2/\text{Al}_2\text{O}_3$ ratios tested at 375 °C, 1 MPa and WHSV of 2 h^{-1}
- Figure 10 TGA curves of the spent catalysts with different $\text{SiO}_2/\text{Al}_2\text{O}_3$ ratios tested at 375 °C, 1 MPa and WHSV of 2 h^{-1}

Figure 1

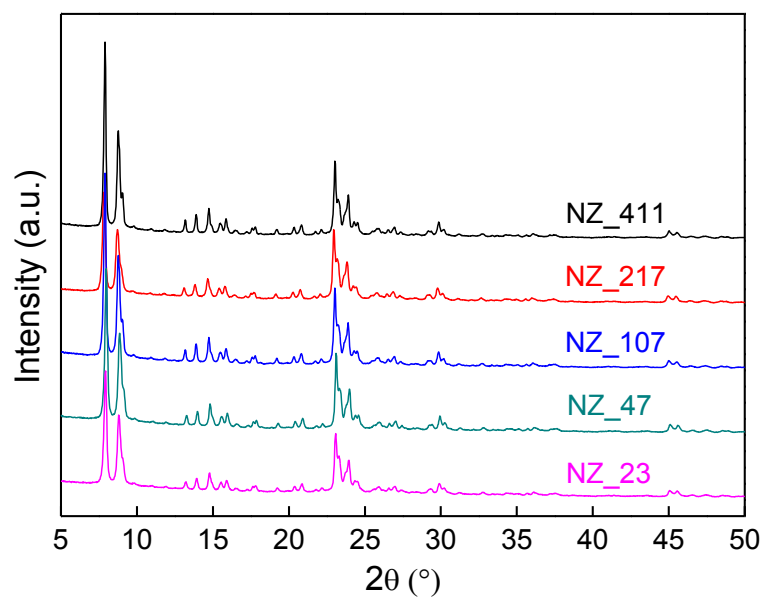


Figure 1 Typical XRD patterns of nanocrystal ZSM-5 samples with various SiO₂/Al₂O₃ ratios ranging from 23 – 411.

Figure 2

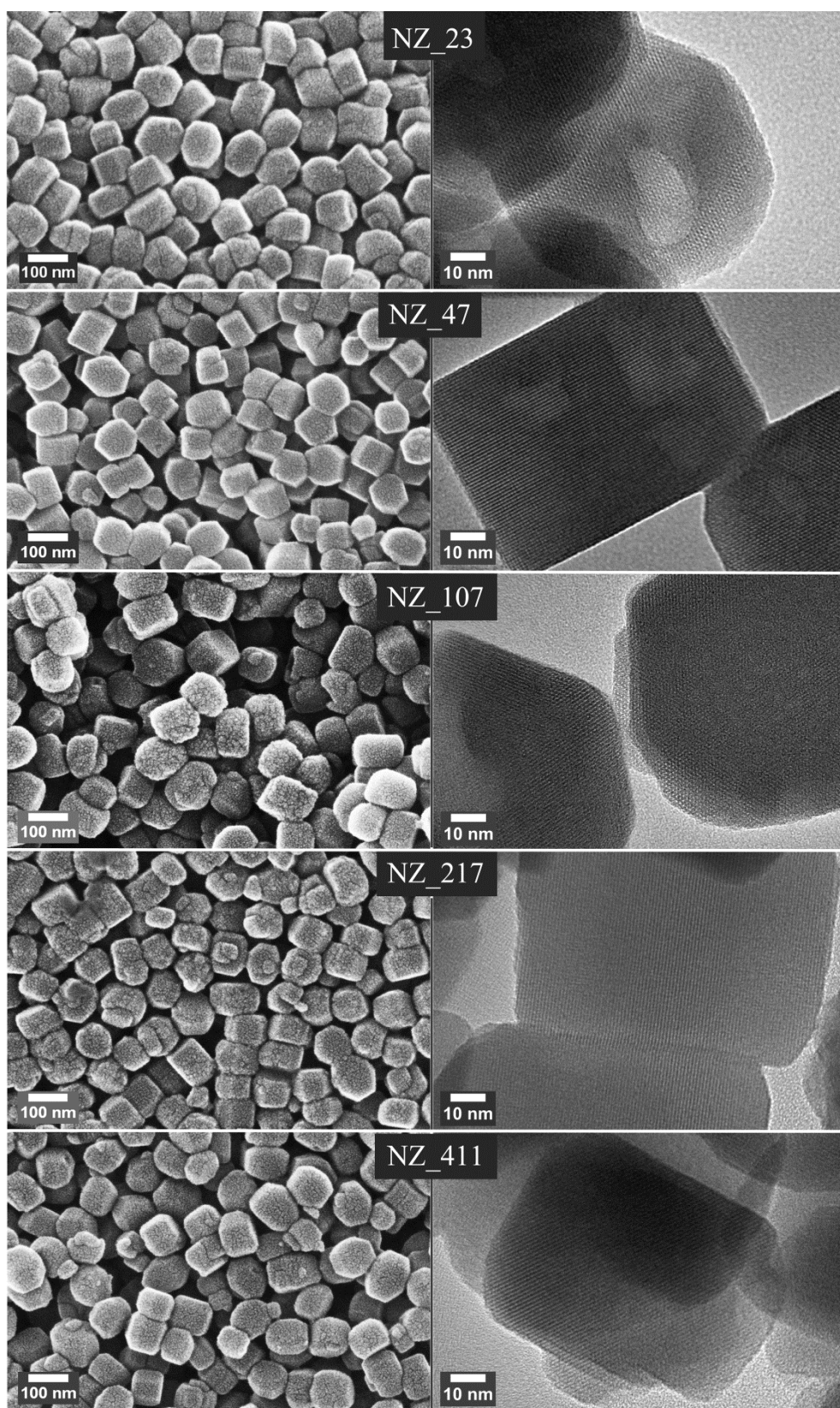


Figure 2 Typical SEM and TEM images of nanocrystal ZSM-5 samples with various $\text{SiO}_2/\text{Al}_2\text{O}_3$ ratios ranging from 23 – 411.

Figure 3

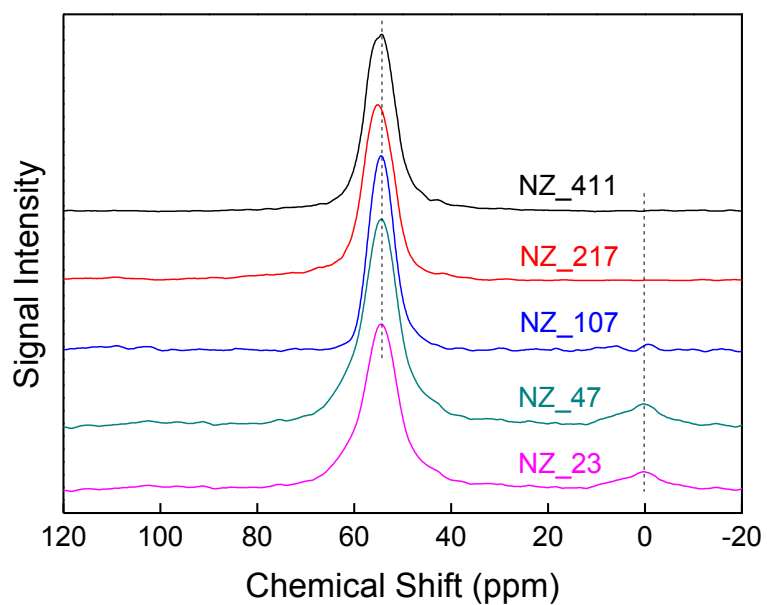


Figure 3 ^{27}Al MAS NMR spectra of nanocrystal ZSM-5 samples with various $\text{SiO}_2/\text{Al}_2\text{O}_3$ ratios ranging from 23 – 411.

Figure 4

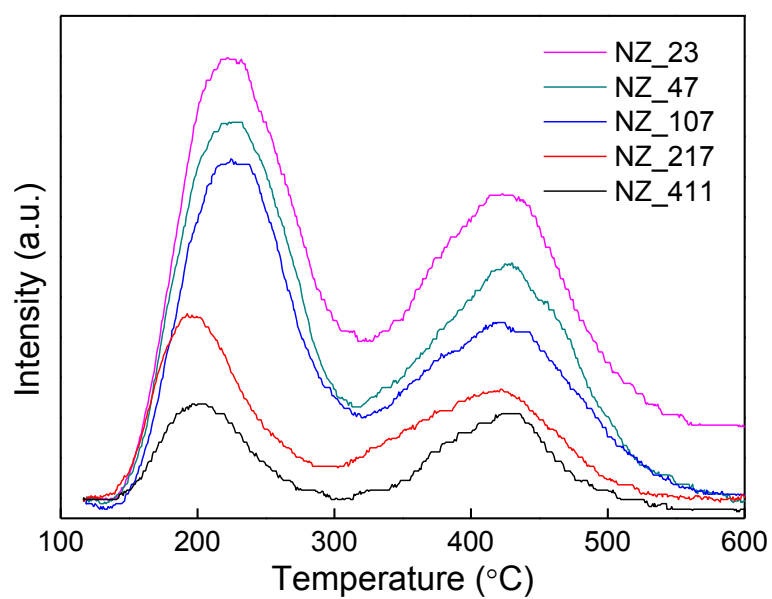


Figure 4 NH_3 -TPD profiles of nanocrystal ZSM-5 samples with various $\text{SiO}_2/\text{Al}_2\text{O}_3$ ratios ranging from 23 – 411.

Figure 5

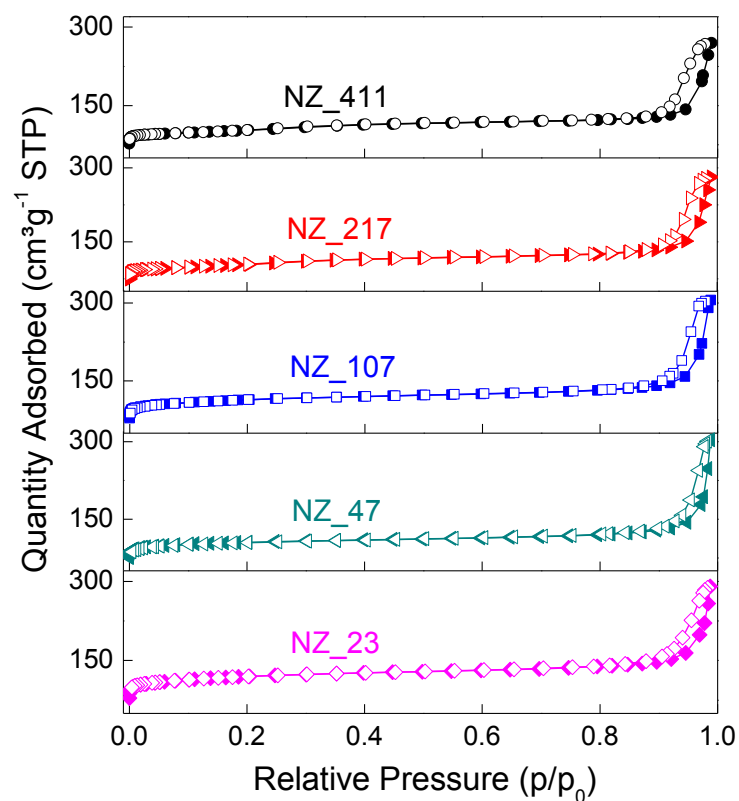


Figure 5 Nitrogen physisorption isotherms of nanocrystal ZSM-5 samples with various $\text{SiO}_2/\text{Al}_2\text{O}_3$ ratios ranging from 23 – 411. Solid symbols denote adsorption and hollow ones for desorption.

Figure 6

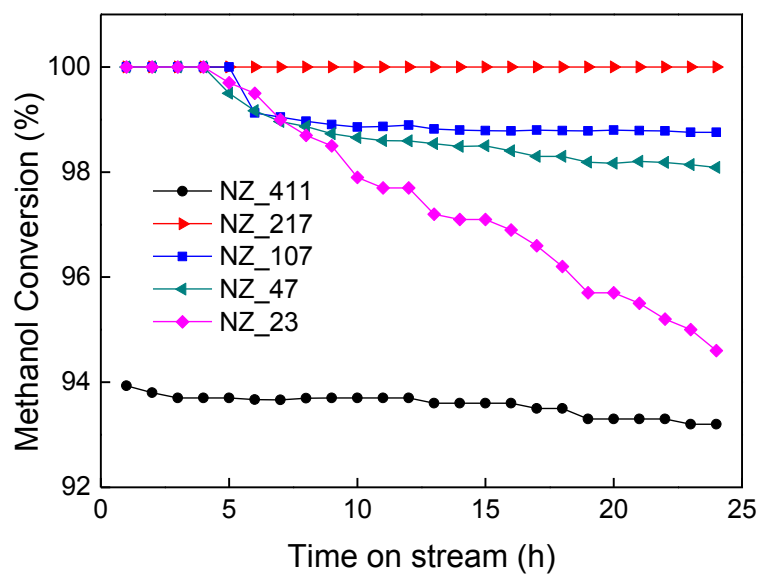


Figure 6 Effect of $\text{SiO}_2/\text{Al}_2\text{O}_3$ ratio on methanol conversion of nanocrystal ZSM-5 zeolite catalysts tested at 375 °C, 1 MPa and WHSV of 2 h^{-1} .

Figure 7

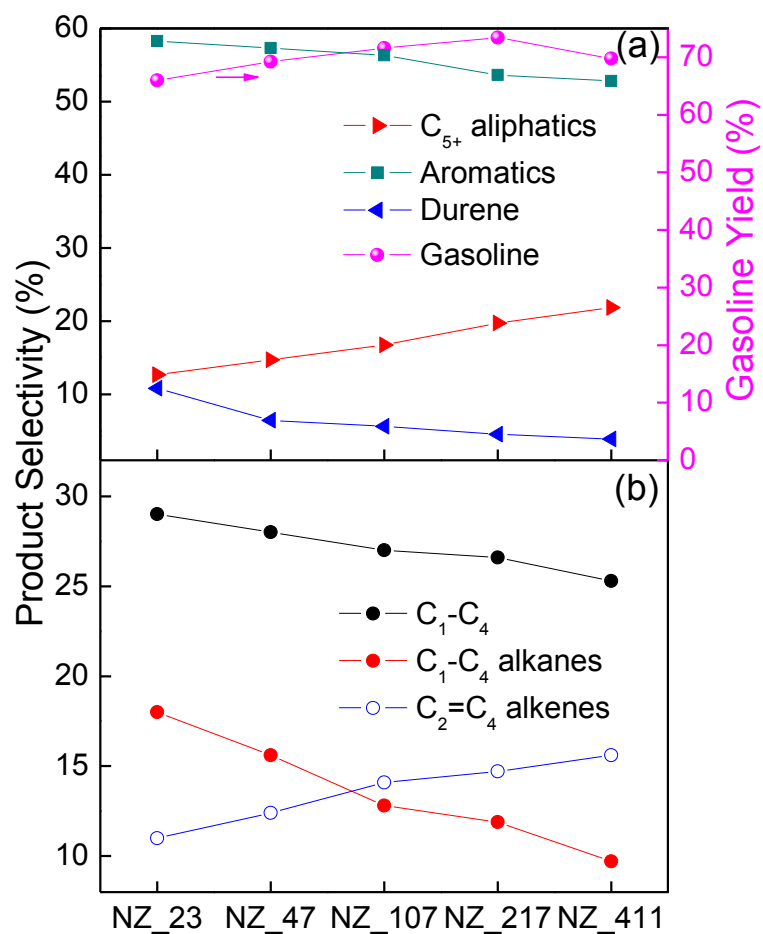


Figure 7 Effect of SiO₂/Al₂O₃ ratio on product distribution and gasoline yield of nanocrystal ZSM-5 zeolite catalysts tested at 375 °C, 1 MPa and WHSV of 2 h⁻¹.

Figure 8

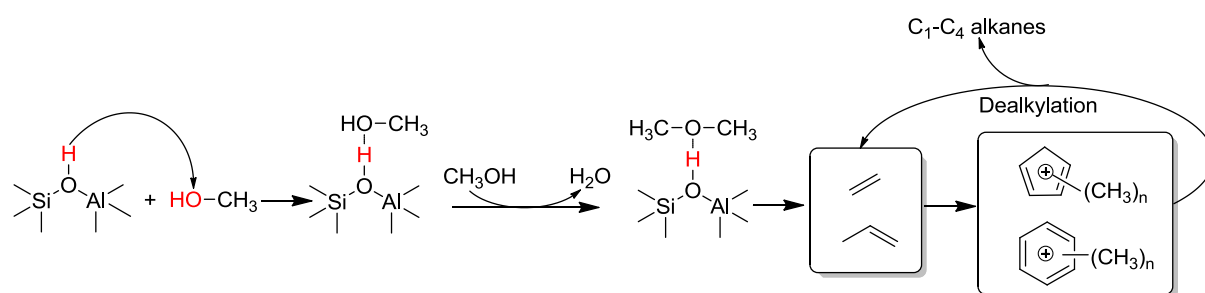


Figure 8 Proposed reaction pathways for methanol conversion on ZSM-5 catalyst.

Figure 9

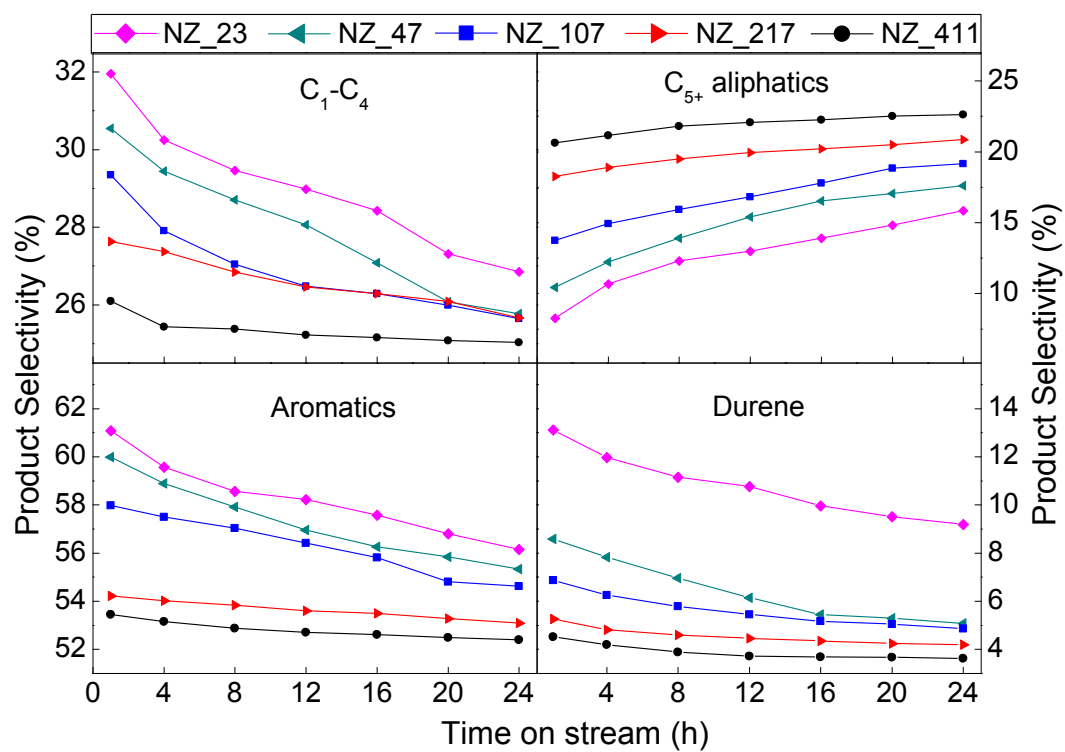


Figure 9 Product selectivity as a function of time for the nanocrystal ZSM-5 zeolite catalysts with various $\text{SiO}_2/\text{Al}_2\text{O}_3$ ratios tested at 375 °C, 1 MPa and WHSV of 2 h⁻¹.

Figure 10

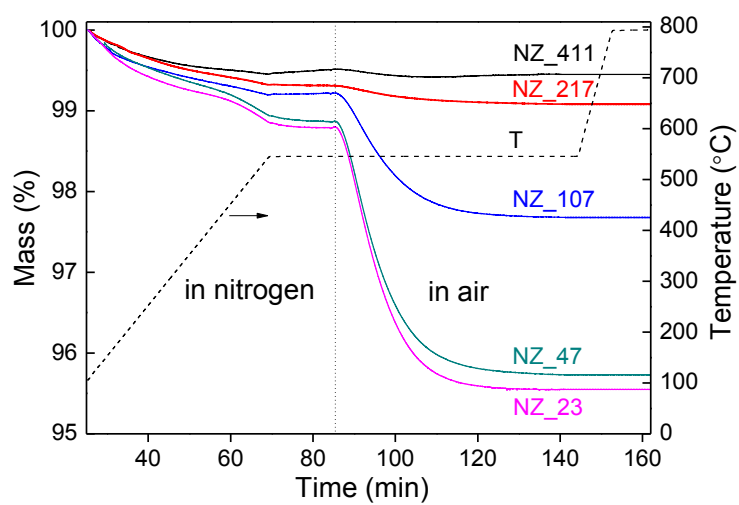


Figure 10 TGA curves of the spent catalysts with different $\text{SiO}_2/\text{Al}_2\text{O}_3$ ratios tested at 375 °C, 1 MPa and WHSV of 2 h^{-1} .

List of Tables

Table 1 Nitrogen physisorption characteristics of nanocrystal ZSM-5 samples with various SiO₂/Al₂O₃ ratios ranging from 23 – 411.

Sample	S_{BET} (m ² g ⁻¹)	t-Plot S_{Micro} (m ² g ⁻¹)	t-Plot S_{Exter} (m ² g ⁻¹)	V_{Total} (cm ³ g ⁻¹)	t-Plot V_{Micro} (cm ³ g ⁻¹)	V_{Meso} (cm ³ g ⁻¹)
NZ_23	418	302	116	0.33	0.12	0.21
NZ_47	420	304	116	0.33	0.12	0.21
NZ_107	426	308	118	0.34	0.13	0.21
NZ_217	430	310	120	0.35	0.13	0.22
NZ_411	435	311	124	0.35	0.13	0.22

Note: S_{BET} = BET surface area, which was calculated using the BET method; t-Plot S_{Micro} = micropore area, which was determined using the t-plot method; t-plot S_{Exter} = external surface area calculated by subtracting the micropore area from the BET area. V_{Total} = total pore volume, which was determined from the adsorbed amount at $p/p_0=0.995$. t-plot V_{Micro} = micropore volume was calculated using the t-plot method; V_{Meso} = mesopore volume was calculated by subtracting micropore volume from the total pore volume.